Understanding Carbon Dioxide Transfer in Direct Methanol Fuel Cells Using a Pore-Scale Model

Nathaniel Metzger
Department of Mechanical Engineering,
University of Kansas,
Lawrence, KS 66046
e-mail: nathanhmetzger@ku.edu

Archana Sekar
Department of Chemistry,
Kansas State University,
Manhattan, KS 66046
e-mail: archanasekar@ksu.edu

Jun Li
Department of Chemistry,
Kansas State University,
Manhattan, KS 66046
e-mail: junli@ksu.edu

Xianglin Li[1]
Department of Mechanical Engineering,
University of Kansas,
Lawrence, KS 66046
e-mail: xianglinli@ku.edu

The gas flow of carbon dioxide from the catalyst layer (CL) through the microporous layer (MPL) and gas diffusion layer (GDL) has great impacts on the water and fuel management in direct methanol fuel cells (DMFCs). This work has developed a liquid–vapor two-phase model considering the counter flow of carbon dioxide gas, methanol, and water liquid solution in porous electrodes of DMFC. The model simulation includes the capillary pressure as well as the pressure drop due to flow resistance through the fuel cell components. The pressure drop of carbon dioxide flow is found to be about two to three orders of magnitude higher than the pressure drop of the liquid flow. The big difference between liquid and gas pressure drops can be explained by two reasons: volume flowrate of gas is three orders of magnitude higher than that of liquid; only a small fraction of pores (<5%) in hydrophilic fuel cell components are available for gas flow. Model results indicate that the gas pressure and the mass transfer resistance of liquid and gas are more sensitive to the pore size distribution than the thickness of porous components. To buildup high gas pressure and high mass transfer resistance of liquid, the MPL and CL should avoid micro-cracks during manufacture. Distributions of pore size and wettability of the GDL and MPL have been designed to reduce the methanol crossover and improve fuel efficiency. The model results provide design guidance to obtain superior DMFC performance using highly concentrated methanol solutions or even pure methanol.
[DOI: 10.1115/1.4050369]

Keywords: direct methanol fuel cell, liquid–vapor two-phase model, pore size distribution, CO_2 flow, water management, methanol crossover, fuel cells

1 Introduction

The mass transfer of carbon dioxide within a direct methanol fuel cell (DMFC) is critical to regulate the mass transfer of fuel (methanol) and water [1–3]. This study focuses on the liquid–vapor two-phase flow of carbon dioxide, methanol, and water within porous electrodes of DMFCs to propose design criteria for DMFCs using concentrated methanol solutions. In DMFCs fed with dilute liquid methanol solutions, the anode methanol oxidation reaction (MOR) oxidizes methanol and water and generates carbon dioxide, while the cathode oxygen reduction reaction (ORR) reduces oxygen and generates water:

$$\text{Anode (MOR): } CH_3OH + H_2O \rightarrow CO_2(g) + 6H^+ + 6e^- \quad (1)$$

$$\text{Cathode (ORR): } 6H^+ + 6e^- + 1.5O_2 \rightarrow 3H_2O \quad (2)$$

$$\text{Overall: } CH_3OH + 1.5O_2 \rightarrow CO_2 \uparrow + 2H_2O \quad (3)$$

The liquid fuel (methanol-water solution) transfers from the fuel channel through the gas diffusion layer (GDL) to the anode catalyst layer (CL) while the generated carbon dioxide gas moves in the opposite direction from the anode CL through the GDL to the fuel channel. Carbon dioxide, methanol, and water have the same molar flux in the anode catalyst layer, determined by the anode MOR reaction Eq. (1). Because carbon dioxide is generated as gas while methanol and water react in the MOR as a liquid, the densities of carbon dioxide gas and methanol solution are different by about 1000 times. As a result, the volume flowrate of carbon dioxide away from the anode catalyst layer is about three orders of magnitude higher than the volume flowrate of the methanol solution into the anode catalyst layer. The counter flow of carbon dioxide and liquid fuel supply has an imperative impact on the fuel supply and crossover rates [4]. Therefore, understanding the pressure change and flowrate of carbon dioxide in fuel cell electrodes (especially in the anode) is critical and will be the focus of this study.

There have been studies to visualize carbon dioxide bubble flow within the fuel channel and to design the anode channels to quickly remove carbon dioxide, especially at high current densities. Yang et al. [5] conducted a detailed study to visualize carbon dioxide bubble flow in a serpentine channel at three different cell orientations: horizontal with the anode facing up, vertical, and horizontal with the anode facing down. The 4 cm^2 DMFC was tested with 1 M methanol solution at 60 °C with a flowrate of 1 ml/min. In addition, carbon dioxide bubble behavior when the methanol flowrates varied from 0.25 to 8.0 ml/min using 1 M methanol was studied and visualized. This study identified the transition from discrete bubbles to gas slugs when the operating current increased. The orientation of the fuel cell was found to have an impact on the performance, especially at low methanol flowrates. Li et al. have designed the anode flow channels of a micro-DMFC with a non-equipotent serpentine flow field [6]. The new flow channel design had a gradient cross-sectional area along the flow direction while keeping the same hydraulic diameter, open ratio, and channel length with the traditional design that uses a uniform cross-sectional area. The micro DMFC reduced the anode pressure drop by half (from 3.21 kPa to 1.65 kPa) at 0.1 A current and less fluctuation of pressure caused by carbon dioxide bubble clogging was seen using the new channel. Previous studies focusing on DMFCs using dilute methanol solutions have indicated that current density has an insignificant impact on the overall mass transfer of methanol and water in the anode of DMFCs and hence the relative low impact on fuel cell performance [7]. Therefore, early model studies focusing on the kinetics of DMFCs assumed that carbon dioxide was dissolved in liquid [8,9] or neglected the convection of methanol solution and carbon dioxide [10]. Most liquid-gas two-phase models of DMFCs neglected the impact of carbon dioxide [11] or indirectly calculated the mass fraction of carbon

[1]Corresponding author.

Manuscript received December 15, 2020; final manuscript received January 25, 2021; published online March 23, 2021. Assoc. Editor: Yinshi Li.

dioxide from the mass fractions of other species so that the summary of the total mass fractions equals unity [12–15]. Only a very small number of models have simulated the CO_2 bubble flow within flow channels [16] and counter flow of carbon dioxide gas and liquid fuel during operation [17]. He et al. [17] considered the counter flow of gas and liquid in the fuel cell GDL using a volume average model. The model quantitatively studied the magnitude of fuel convection and diffusion. The pressure distributions of liquid and gas, which drive gas and liquid flow within the GDL, were calculated in the model. Convection was found to be relatively small, compared with diffusion, in transport fuel to the catalyst layer. We are not aware of a model study that simulates liquid-gas two-phase counter flow in a DMFC taking the pore size effect on capillary pressure into consideration. Therefore, this study can fill the knowledge gap to understand the impact of pore-scale capillary pressure on liquid fuel and carbon dioxide gas transfer. Designs of fuel cell structures have also been proposed based on the model to enable DMFCs using highly concentrated methanol solution or pure methanol.

2 Model Description

2.1 Computational Domain. Figure 1 shows the one-dimensional physical domains of a typical membrane electrode assembly (MEA), which consists of a pair of GDLs, microporous layers (MPLs), and CLs on both sides of a polymer electrolyte membrane (PEM). The MEA is sandwiched between two parallel flow fields. A liquid-vapor two-phase mass transport model was developed to investigate the multi-physics phenomena in the MEA. The pore size distribution of the GDL and MPL was derived from the literature. The geometric dimensions and some model parameters of the DMFC are listed in Table 1.

2.2 Model Assumptions

- The anode fuel channel is supplied with only liquid methanol solutions.
- The gas escape from the MEA to the fuel channel is only carbon dioxide; the partial pressure of water vapor and methanol vapor are negligible compared with the total gas pressure.
- The fuel cell has a uniform temperature of 80 °C everywhere.
- Porous media can be simplified as a bundle of microcylinders with the same contact angle but different diameters.
- The gravity force is negligible. The Bond number, defined as the ratio between the gravitational force over the surface tension force ($\rho g d^2/\sigma$), in porous structures with a pore size of 10 μm is on the order of 10^{-3}. This extremely low Bo number indicates that the gravitational force is negligible on such small length scale and can be neglected.
- The catalyst layer is thin, and the generated carbon dioxide uniformly fills the CL. The pressure difference within the CL is negligible.

2.3 Pore Size Distribution. This study assumes that the pore size distributions in porous fuel cell electrodes following lognormal distributions with different mean pore sizes and shape factors [18]. The probability of pore size of x in a fuel cell component follows the following probability distribution function (PDF):

$$\mathrm{PDF}(x) = \exp\left[\frac{-(\ln x - d_{\mathrm{mean}})^2}{2\sigma^2}\right] \Big/ \left(\sqrt{2\pi}\cdot\sigma x\right) \text{ for } x > 0 \quad (4)$$

where the mean pore size d_{mean} and the shape factor σ can be estimated from experimental data reported in the literature [19]. Then the fraction of pores with a diameter of x or smaller can be calculated using the following cumulative distribution function:

$$\mathrm{CDF}(x) = \frac{1}{2} + \frac{1}{2}\mathrm{erf}\left(\frac{\ln x - d_{\mathrm{mean}}}{\sqrt{2}\sigma}\right) \text{ for } x > 0 \quad (5)$$

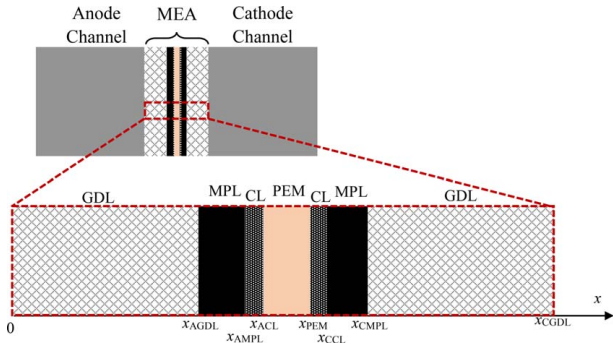

Fig. 1 Schematic of the computational domain (1D model)

Table 1 Properties of MEA components in this model [20]

	Thickness δ (μm)	Mean pore size d_{mean} (μm)	Shape Factor σ (/)	Porosity ε (/)	Contact angle θ (deg)	Permeability K (m^2)
GDL	200	10	1.0	0.8	50 [21]	3×10^{-12}
MPL	50	0.1	1.0	0.3	70	7×10^{-13}
CL	20	0.1	1.0	0.2	30	3×10^{-14}
PEM	50	0.01	1.0	0.2	25 [22]	7.13×10^{-20} [23]

The mean pore size, the shape factor, and other properties of fuel cell components are summarized in Table 1.

2.4 Governing Equations

2.4.1 Gas Pressure Drop. The surface tension of the methanol–water mixture varies significantly with temperature and methanol concentration [24]. The mass fraction of methanol is 3.3% and 10.9% when the methanol concentration is 1 and 3 M, respectively. The surface tension of the 1M methanol solution at 80 °C is estimated to be 50 mN/m. Assuming the liquid can wet all MEA components, including the MPL, the gas (carbon dioxide) pressure that breaks through cylindrical pores filled with liquid is determined by the capillary pressure:

$$p_{\mathrm{C}} = p_{\mathrm{g}} - p_{\mathrm{l}} = \frac{4\cdot\gamma\cdot\cos\theta}{d} \quad (6)$$

Assume the liquid pressure is the atmospheric pressure, p_0, the gas pressure that is required to break through pores with diameter d is

$$p_{\mathrm{g}} = p_0 + \frac{4\cdot\gamma\cdot\cos\theta}{d} \quad (7)$$

where γ is the surface tension of the liquid, 50 mN/m, and θ is the contact angle between the liquid and gas on the solid surface. Once the gas bubble breaks through the pore, the pressure drop of the gas flow through the MPL and GDL can be determined by the permeability and volume flowrate following the Kozeny–Carman equation:

$$\frac{\Delta p_g}{\delta} = -\frac{150\mu}{d_{avg,g}^2}\frac{(1-\varepsilon)^2}{\varepsilon^3}v_s \quad (8)$$

where $d_{avg,g}$ is the average diameter of pores larger than d (which are filled with gas), μ is the dynamic viscosity of carbon dioxide gas, 1.755×10^{-5} Pa s, and ε is the porosity. It should be noted that the sphericity is assumed to be unity in this study. The superficial velocity $v_{s,g}$ is calculated by the volumetric gas

flowrate, Q_g, and the cross-sectional area that have gas flow:

$$v_{s,g} = \frac{Q_g}{A \times (1 - \mathrm{CDF}(d))} \tag{9}$$

Since gas can only go through pores with a size larger than d, the area of the gas flow is calculated by $A \times (1 - \mathrm{CDF}(d))$, where $\mathrm{CDF}(d)$ is the cumulative distribution function at pore size d. The volume flowrate of carbon dioxide per projected area of the MEA is proportional to the operating current density i:

$$\frac{Q_g}{A} = \frac{i}{6F} \times \frac{R_u T}{p_g} \tag{10}$$

where F is the Faraday constant, 96,485 C/mol, R_u is the universal gas constant, 8.314 J/mol/K, and p_g is the gas pressure. Therefore, the pressure drop through the thickness direction (δ is the thickness) of the fuel cell component, Δp_g, can be calculated by

$$\frac{\Delta p_g}{\delta} = -\frac{150\mu}{d_{avg,g}^2} \frac{(1-\varepsilon)^2}{\varepsilon^3} \times \frac{i}{6F} \times \frac{R_u T}{p_g} \times \frac{1}{(1 - \mathrm{CDF}(d))} \tag{11}$$

The total gauge pressure of carbon dioxide in the catalyst layer includes the breakthrough pressure of the bubbles (Eq. (7)) and the pressure drop of the gas flow (Eq. (11)):

$$\Delta p_{g,tot} = \frac{4 \cdot \gamma \cdot \cos\,\theta}{d} + \frac{150\mu}{d_{avg,g}^2} \frac{(1-\varepsilon)^2}{\varepsilon^3} \times \frac{i}{6F} \times \frac{R_u T}{p_g} \times \frac{\delta}{(1 - \mathrm{CDF}(d))} \tag{12}$$

Applying Eq. (12) to different porous fuel cell components, which have different pore size distribution and wettability, can result in a balanced pressure with the operating current density.

2.4.2 Liquid Pressure Drop. The flow pressure drop of liquid flow through porous media, Δp_g, can be calculated by

$$\frac{\Delta p_l}{\delta} = \frac{150\mu}{d_{avg,l}^2} \frac{(1-\varepsilon)^2}{\varepsilon^3} v_{s,l} \tag{13}$$

where $d_{avg,l}$ is the average diameter of pores smaller than d (which are filled with liquid). The superficial velocity is calculated by the volumetric liquid flowrate, Q_l, and the cross-sectional area that have gas flow:

$$v_{s,l} = \frac{Q_l}{A \times \mathrm{CDF}(d)} \tag{14}$$

The volumetric flowrate of liquid (methanol and water) per projected area of the MEA is proportional to the operating current density i:

$$\frac{Q_l}{A} = \frac{i \times (M_{\mathrm{H2O}} + M_{\mathrm{MeOH}})}{6F} \Big/ \rho_l \tag{15}$$

Therefore, the liquid pressure drop through the thickness direction of the fuel cell component can be calculated by

$$\Delta p_l = \frac{150\mu}{d_{avg}^2} \frac{(1-\varepsilon)^2}{\varepsilon^3} \times \frac{i \times (M_{\mathrm{H2O}} + M_{\mathrm{MeOH}})}{6F\rho_l} \times \frac{\delta}{\mathrm{CDF}(d)} \tag{16}$$

2.5 Experiments to Validate the Model. This study has also conducted experiments to measure the pressure change during fuel cell operation to validate the model. The anode gas diffusion electrode (GDE) was fabricated by airbrush spraying PtRu/C (32.8:16.9:50.3) catalysts (TEC 66E50—Tanaka Kikinzoku Kogyo K.K.) dispersed in ionomer-containing ethanol (at about 2 mg catalyst per milliliter of ethanol) on Toray TGP-H-60 carbon paper at 70 °C on a hotplate and the cathode GDE was made by spraying Pt/C(60:40) (HiSPEC® 9100—Johnson Matthey) catalysts on TGP-H-60 carbon paper in a similar way. The anode catalyst loading was 4.4 $\mathrm{mg_{PtRu}/cm^2}$, and the cathode catalyst loading was 1.2 $\mathrm{mg_{Pt}/cm^2}$. The ionomer to total catalyst ratio was 0.2 in the anode GDE and the ionomer to carbon ratio was 1 in the cathode GDE. The anode and cathode GDEs were then hot-pressed with a pre-treated Nafion 212 membrane at 135 °C (275 F) and 0.345 MPa (50 psi) for 5 min to make the MEA. After activation using 0.25 M methanol and air, polarization curves of activated MEAs were tested at 80 °C with 1 M (0.1 ml/min) methanol solutions and fully hydrated air (0.1 l/min with 50 kPa back pressure) using a Scribner Associates 890e 500W 50/125/250A Fuel Cell Test System. The methanol and air supply rates were controlled by a PeriWave Milliþ5 pump (CorSolutions) with 10 μl/min accuracies and a Cole-Parmer mass flow controller with 2.5 ml/min accuracy. Air from a compressed air cylinder was fully humidified at 80 °C before being supplied to the fuel cell. In addition to the performance test, this study has also applied two pressure transducers (PX409-050GUSBH—Omega) with ±0.5% full-scale accuracy both near the exit of flow channels to measure the pressure variations in the anode and cathode when the fuel cell operated at different current densities. Details of the experimental setup can be found in our recent publication [25].

3 Model Comparisons

3.1 Model With Constant Pore Size and Wettability. In the model that assumes a constant pore size and wettability in each component, the pressure drop at a given current density (Eq. (12)) will be reduced to

$$\Delta p_{g,tot} = \frac{4 \cdot \gamma \cdot \cos\,\theta}{d} + \frac{150\mu}{d_{avg}^2} \frac{(1-\varepsilon)^2}{\varepsilon^3} \times \frac{i}{6F} \times \frac{R_u T}{p_g} \times \delta \tag{17}$$

The capillary pressure for the bubble to break through the hydrophilic pores and pressure drop due to the volume flowrates at 0.1 A/$\mathrm{cm^2}$ are compared in Table 2. It could be seen that the pressure drop due to flow resistance is negligible (more than two orders of magnitude smaller) compared with the capillary pressures in GDL, MPL, and CL. While the flow resistance is higher than the capillary pressure in the PEM. Because the flow resistance changes faster (proportional to d^{-2}) than the capillary pressure (proportional to d^{-1}) with the pore size (d), the flow resistance is significant in components with extremely small pore size such as the PEM. The constant-pore-size model underestimates the pressure drop due to gas flow because of the assumption that all pores are available for gas transfer. Meanwhile, the constant-pore-size model overestimates the capillary pressure for the gas to break through pores without considering the fact that gas prefers to go through large pores with lower capillary pressure.

Figure 2 shows a sketch of liquid–gas two-phase flow through porous fuel cell components. The porous structure of the MPL has been simplified into bundles of microtubes with various diameters. Since the MPL is hydrophilic to the methanol–water solution, with a contact angle of 70 deg, the liquid is the wetting phase that can invade the MPL by capillary pressure. The pressure of the gas phase, which is the non-wetting phase, must be higher than the local capillary pressure in order to break through the liquid-filled pores (Eq. (6)). Even though the mean pore size of the MPL is

Table 2 Pressure drop across various fuel cell components with constant pore size

	Total (Pa)	Capillary pressure (Pa)	Flow pressure (Pa)
GDL	1.3×10^4	1.3×10^4	1.7×10^{-2}
MPL	6.9×10^5	6.8×10^5	1.0×10^4
CL	1.7×10^6	1.7×10^6	1.8×10^4
PEM	6.3×10^7	1.8×10^7	4.5×10^7

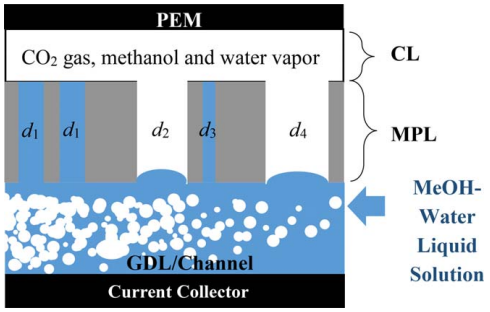

Fig. 2 Schematic of liquid–gas two-phase flow through the anode fuel cell components

estimated to be 0.1 μm, which has a capillary pressure of 6.8×10^5 Pa, larger pores and cracks in the MPL have lower capillary pressure. Therefore, carbon dioxide gas will first burst through large pores and cracks in the MPL, demonstrated in Fig. 2. The breakthrough pressure of carbon dioxide gas is much lower than the capillary pressure estimated by the mean pore size. But this phenomenon cannot be captured by models assuming a constant pore size. In order to have a continuous gas flow, the gas pressure must be higher than the summary of the capillary pressure and pressure drop due to flow resistance (Eq. (12)). The following pore-scale model can consider these factors and generate more accurate results.

3.2 Model With Distributions of Pore Size. The pore-scale model considers the pore size distribution within porous components (Fig. 3(*a*)). Both the capillary pressure and the pressure caused by flow resistance are highly dependent on the pore size distribution. Figure 3(*b*) shows an example of the capillary pressure and the flow pressure drop through an MPL with log-normal pore size distribution when the operating current density is 0.1 A/cm^2. The capillary pressure decreases with the increase of the cutoff pore size (pores larger than the cutoff pores are available for gas flow) following Eq. (6). Meanwhile, the pressure drop introduced by flow resistance increases with the increase of the cutoff pore size. A larger cutoff pore size results in higher cumulative distribution function in Eq. (11) and fewer pores available for gas flow. Even though the flow resistance is smaller in each large pore, there are a much smaller number of large pores available for the gas flow. As a result, the flow pressure increases with the increase of cutoff pore size. The resulting total pressure, which is the sum of the capillary pressure and pressure drop, reaches a minimum of 2.6×10^5 Pa at the cutoff pore size of about 0.33 μm in the MPL at the current density of 0.1 A/cm^2. Based on the log-normal distribution of pore size, only a small fraction of pores (12%) are filled by gas while the rest of pores with a diameter of 0.33 μm or smaller are filled by a liquid solution. Similar trends of the total pressure are obtained in other components (GDL, CL, and PEM) with different minimum pressures and cutoff pore sizes to obtain the minimum pressure.

The total pressure drops at different current densities are compared in Fig. 4. Values of pressure change by capillary pressure and flow pressure drop are also compared in Table 3. Please note that the pressure drop in Fig. 4 and Table 3 are the minimum total pressure drop balancing the capillary pressure and pressure drop by flow resistance. The pressure increases with the increase of current density in all components since the gas generation rate increases linearly with the increase of current density. The pressure drop is very high through the PEM because of its extremely small pore size and low contact angle. The pressure drop through the GDL is negligible comparing with the pressure drop across the MPL and CL since the pore size in the GDL is roughly two orders of magnitude larger than the pore size in the MPL and CL. In order to regulate the gas flow and the flow of liquid methanol and water, efforts should be focused on engineering the MPL.

3.3 Model Validations. According to the previous discussions, the pressure increases with the operating current density because of the higher generation rate of carbon dioxide gas. When the liquid and gas are in equilibrium in porous fuel cell components (Fig. 2) the experimentally measured pressure changes using the pressure transducer indicate the pressure drop required to drive gas through the fuel cell components (mainly the GDL and MPL). Although the total gas pressure in the CL is high, the pressure measured in the flow channel has been significantly reduced by the high capillary pressure through the MPL and GDL. The gas pressure at various current densities measured by the pressure transducer and model predictions are shown in Fig. 5. Error bars in Fig. 5 were calculated from four sets of experimental data. The prediction using the liquid-vapor pore-scale model matches with experimental measurements with an average error of 23%. The discrepancy between simulation and data is partially caused by the simplification of the porous structure to bundles of straight tubes in the model. Nevertheless, the trend and magnitude of pressure change predicted by the mode have a good agreement with experimental data. The following results and discussions are derived based on the model with pore size distributions in each fuel cell component.

4 Results and Discussions

4.1 Gas and Liquid Pressure Distributions in Membrane Electrode Assembly. The pressure drops of gas flow across different components when the current density is 0.1 A/cm^2 are illustrated in Fig. 6. Distributions at other current densities follow a similar trend. Due to the high flow resistance, the generated

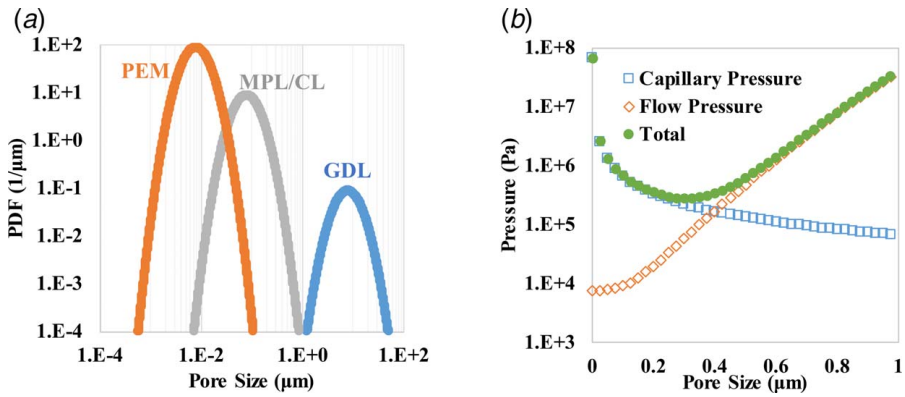

Fig. 3 (*a*) Pore size distributions of different fuel cell components and (*b*) the capillary

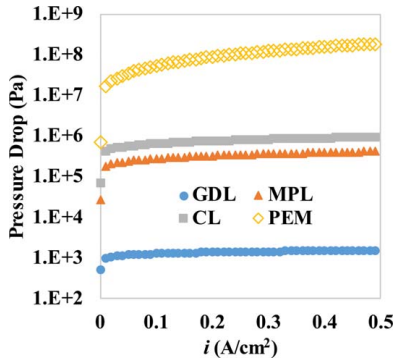

Fig. 4 Total pressure drops across each component at different operating current densities

Table 3 Pressure breakdowns of the pore size distribution model at 0.1 A/cm^2

	Total gas pressure (Pa)	Capillary pressure (Pa)	Gas flow pressure (Pa)
GDL	5.1×10^{2}	5.1×10^{2}	5.1×10^{-2}
MPL	5.2×10^{4}	3.5×10^{4}	1.7×10^{4}
CL	1.2×10^{5}	8.1×10^{4}	3.7×10^{4}
PEM	1.9×10^{7}	4.6×10^{6}	1.4×10^{7}

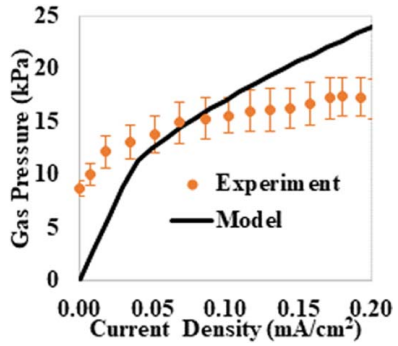

Fig. 5 Variations of gas pressure with operating current density

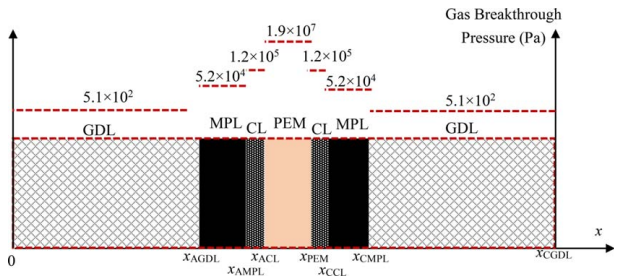

Fig. 6 Pressure drop of gas flow through different fuel cell components at the current density of 0.1 A/cm^2

carbon dioxide in the anode CL cannot cross-over the PEM and must move across the MPL and GDL to the anode fuel channel. Most fuel cell components and the majority of pores are hydrophilic to methanol solutions. As a result, liquid fuel can be automatically delivered to the CL through capillary force. The mass transfer of liquid to the catalyst is sufficiently quick to provide enough fuel and water to reaction sites. The un-reacted methanol and water will cross-over from the anode CL through the strongly hydrophilic PEM and reach the cathode CL.

4.2 Impact of the Shape Factor of Pore Size Distribution. The shape factor has a significant impact on the pore size distribution and hence the mass transfer properties of fuel cell components. This section quantitatively compares the gas pressure drop across fuel cell components when the shape factor changes between 1 and 0.25. Reducing the shape factor will lead to a narrower range of pore sizes. When the shape factor approaches 0, the log-normal distribution approaches a constant pore size.

Results in Fig. 7(*a*) show that the gas pressure drops are lower when the pore size has a wider distribution (larger shape factor). Capillary pressure and the flow pressure drop are both lower in larger pores. Gas as the non-wetting phase tends to flow through larger pores and the model results show that gas only fills less than 1% of pores (larger) in the GDL, MPL, and CL at 0.1 A/cm^2. As a result, the porous components with wider distributions of pore size have lower resistance for gas flow and hence lower pressure drop. Comparisons between experimental data and model results using different shape factors in Fig. 7(*b*) indicate that pressure drops simulated using a shape factor of 1 result in better agreements with experimental results. The pressure drop of gas flow is over-estimated based on pore size distributions with smaller shape factors. On the contrary, the model using constant pore size underestimated the pressure drop since this model assumes that all pores are available for gas flow. Shape factors of fuel cell components can be engineered during the fabrication of the MEA components using raw materials with different sizes, amounts of binding material, compression pressures, etc. In addition, results also indicate that the amount and size of microcracks in MPLs and CL can dramatically change the shape factor and overall mass transfer properties.

4.3 Impact of Component Thickness. Another important designing parameter is the thickness of fuel cell components. This study simulated the pressure drop of gas flow through the MPL with different thicknesses in Fig. 8. The total pressure drops through the MPL only changes between 42 kPa and 86 kPa at 0.1 A/cm^2 and between 60 kPa and 140 kPa at 0.3 A/cm^2 when the MPL thickness increases from 25 to 200 μm (Fig. 8(*a*)). As a comparison, the total pressure drops change between 52 kPa to 293 kPa and then 537 kPa when the shape factor of the MPL changes from 1 to 0.5 and then 0.25 (Fig. 8(*b*)) at 0.1 A/cm^2. These results show that changing the pore size distribution and minimizing the micro cracks is more effective than changing the thickness to regulate the liquid and gas flow in MEAs.

4.4 Designs of Membrane Electrode Assembly Structures to Reduce Fuel Crossover. In order to reduce the methanol crossover when highly concentrated methanol solutions are used, the MEA design needs to consider the impact of capillary pressure to increase the gas pressure escaping the CL or reduce the capillary pressure of liquid flow into the CL. The following designs are proposed and compared by the model to quantify the gas and liquid flow resistance within MEA. The capillary pressure of micro-meter-size pores is much higher than the liquid flow resistance, and the time scale for contact angle dynamics is on the order of 1–10 ms [26]. Therefore, the design principle is to reduce the liquid connection between the CL and the fuel channel.

The first design includes a strongly hydrophilic layer between the MPL and the GDL (Fig. 9(*a*)). The hydrophilic layer has similar wettability and pore size with the catalyst layer and can build a pressure gradient to trap the liquid fuel between the CL and the channel using capillary pressure. This layer serves as a sink for methanol fuel to reduce the methanol crossover across the PEM. The second design includes an electric-conductive porous structure with very large pores (~mm) between the MPL and the CL. The

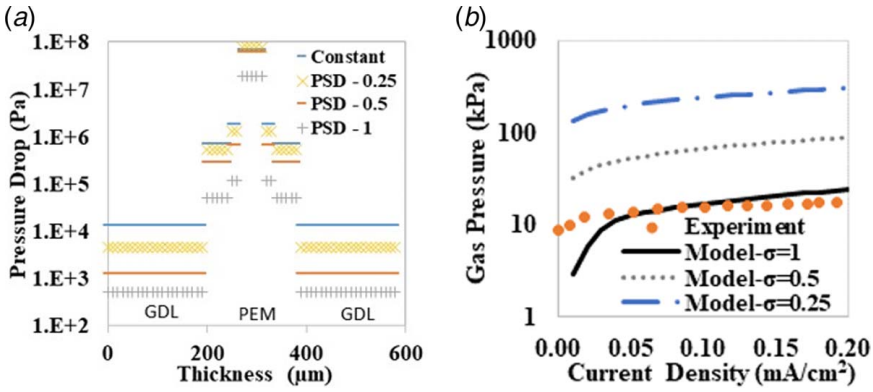

Fig. 7 (*a*) Total gas pressure drop (capillary pressure + flow pressure drop) through different parts of the fuel cell at the current density of 0.1 A/cm^2 and (*b*) simulated and experimentally measured gas pressure change with the operating current density

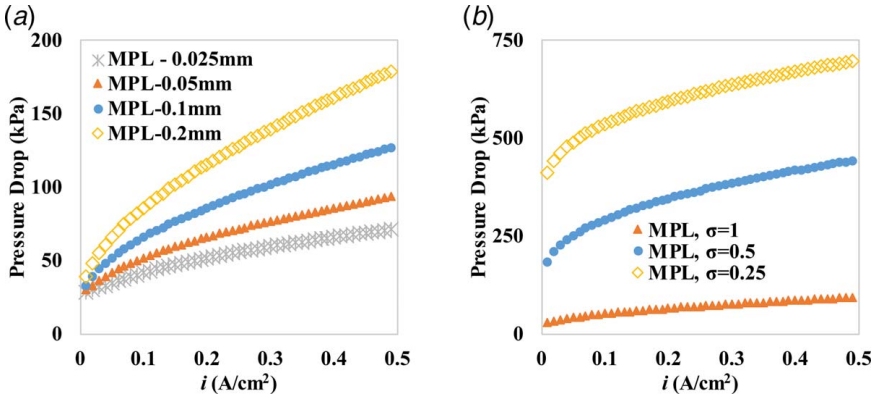

Fig. 8 Total gas pressure drops through MPLs with (*a*) different thicknesses at the shape factor of 1.0 and (*b*) different shape factors at the thickness of 50 μm

pore size in this structure (labeled as large pores in Fig. 9(*b*)) is much larger than those in the MPL and CL so it has negligible capillary pressure and can easily be filled by carbon dioxide gas. As a result, this structure (gap) can serve as a gas trap and reduce the methanol crossover. The third design in Fig. 9(*c*) uses a strongly hydrophilic MPL instead of the traditional hydrophobic MPL. This hydrophilic MPL can be made from mixtures of carbon and Nafion to have a contact angle similar to that of the PEM (25 deg in this study). The strongly hydrophilic MPL has extremely high capillary pressure so the breakthrough pressure of the carbon dioxide gas generated in the CL is high. The high gas pressure in the CL will increase the liquid flow resistance and can reduce the methanol crossover rate. The following discussions will quantitatively analyze the mass transfer in these different designs of MEAs.

In the first design in Fig. 9(*a*), if the hydrophilic layer has similar properties with the CL, carbon dioxide gas needs to build up a pressure of at least 1.2×10^5 Pa at 0.1 A/cm^2 to go across this hydrophilic layer. When the gas pressure is 1.2×10^5 Pa in the MPL, 4.1% of pores (with pore size larger than 0.57 μm) in MPL are filled by gas where the rest of the pores (smaller than 0.57 μm) are filled by a liquid solution. As a result, the resistance of liquid transfer is increased, and the fuel and water crossover could be reduced. Comparing with the baseline case without this hydrophilic layer, the liquid pressure drop to go through the MPL is increased from 1.8×10^2 Pa to 7.0×10^2 Pa. In this case, most pores connected with CL are still filled by liquid. If the hydrophilic membrane has an even lower contact angle or pore size, carbon dioxide gas needs to build up even higher pressure to transfer through the MPL. For instance, when the gas pressure is 2.5×10^6 Pa in the MPL, more than 90% of pores (with pore size larger than 0.027 μm) in MPL are filled by gas where the rest of the pores (smaller than 0.027 μm) are filled by a liquid solution. Since very limited pores (less than 10%) are available for liquid flow, the liquid mass transfer resistance is extremely high so that the fuel and water crossover are significantly reduced. The liquid pressure drop to go through the pores smaller than 0.027 μm in MPL is calculated to be 3.7×10^5 Pa.

In the second design in Fig. 9(*b*), carbon dioxide gas can easily fill up the whole gap between the MPL and CL. As a result, the mass transfer resistance of the liquid transfer is much larger due to the lack of capillary pressure. The liquid must evaporate to go through the gap and then condense within the CL for the reaction to occur. This design is similar to the concept of passive DMFCs applying a Nafion membrane between the fuel channel (or tank) and the GDL to evaporate methanol when highly concentrated methanol solutions are used as the fuel [27]. Methanol solutions cannot transfer through the evaporation (Nafion) membrane due to the extremely high capillary pressure of a liquid. As a result, the methanol solution must evaporate in order to go through the GDL and reach the CL. The first and second designs may result in similar fuel and water reduction results, but the mechanisms are different. The first design increases the gas pressure to reduce the number of pores filled by liquid that connects to the CL. The second design has much lower gas pressure in the CL and reduces the liquid flow by significantly decreasing the capillary pressure that connects the GDL with the CL.

In the third design in Fig. 9(*c*), the MPL is strongly hydrophilic. The contact angle of the MPL is similar to the PEM (25 deg). Because the MPL is more hydrophilic, the capillary pressure of gas flow is higher. The calculated pressure drop across the MPL at 0.1 A/cm^2 is 1.26×10^6 Pa (similar to the pressure across the CL) or higher. The pressure drop due to liquid flow across the

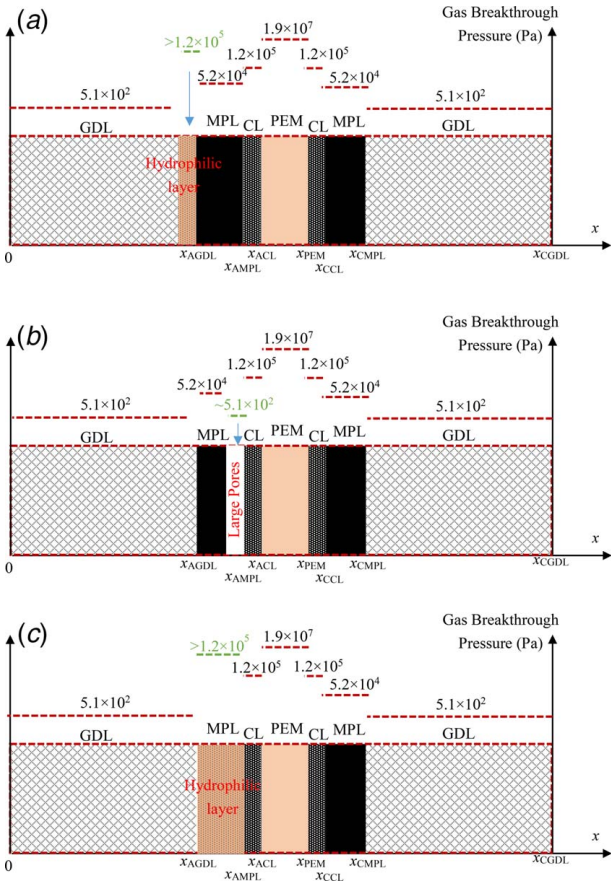

Fig. 9 Pressure drop of gas flow through two new fuel cell structures with (*a*) a hydrophilic layer between GDL and MPL and (*b*) a gap or porous structure with a large pore size

MPL at 0.1 A/cm^2 is increased to 7.2×10^2 Pa. If the MPL is further pressed to have a smaller pore size (mean pore size of 0.05 μm), the pressure drop of the gas flow is further increased to 2.7×10^6 Pa at 0.1 A/cm^2. The calculated liquid pressure drop across the MPL at 0.1 A/cm^2 is further increased to 3.0×10^3 Pa.

4.6 Impact of Current Density (0.3 A/cm^2). In the first design in Fig. 9(*a*), if the hydrophilic layer has similar properties with the CL, carbon dioxide gas needs to build up a 1.7×10^5 Pa pressure at 0.3 A/cm^2 to go across this hydrophilic layer. When the gas pressure drop is 1.7×10^5 Pa in the MPL, 8.2% of pores (with pore size larger than 0.4 μm) in the MPL are filled by gas where the rest of the pores (smaller than 0.4 μm) are filled by a liquid solution. As a result, the resistance of liquid transfer is increased, and the fuel and water crossover could be reduced. Comparing with the baseline case without this hydrophilic layer, the liquid pressure drop to go through the MPL is increased from 5.2×10^2 Pa to 9.3×10^2 Pa.

In the third design in Fig. 9(*c*), the MPL is strongly hydrophilic. The contact angle of the MPL is similar to the PEM (25 deg). Because the MPL is more hydrophilic, the capillary pressure of gas flow is higher. The calculated pressure drop across the MPL at 0.3 A/cm^2 is 1.4×10^6 Pa (similar to the pressure across the CL) or higher. The calculated liquid drop across the MPL at 0.3 A/cm^2 is increased from the base case of 5.2×10^2 to 2.15×10^3 Pa. If the MPL is further pressed to have a smaller pore size (mean pore size of 0.05 μm), the pressure drop of the gas flow is further increased to 3.2×10^6 Pa at 0.3 A/cm^2. The calculated liquid pressure drop across the MPL at 0.3 A/cm^2 is increased to 9.15×10^3 Pa.

5 Conclusion

The mass transfer of carbon dioxide is critical to understand and regulate the fuel and water crossover in DMFCs. We developed a simple liquid–vapor two-phase model to simulate the counter flow of carbon dioxide gas and liquid methanol solution during fuel cell operation. Even though this study did not consider the non-isotropic properties of the porous fuel cell component [28] and the tortuosity of the porous media, a clear understanding of multi-phase flow in straight tubes derived from this work is necessary to understand mass transfer in more complicated geometries. Results and conclusions developed by this study can be easily applied to tortuous porous media with corrections of tortuosity. Several MEA designs have been proposed and analyzed based on this model to enable DMFCs driven by highly concentrated methanol solutions or even pure methanol. The main conclusions from this study include:

(1) The pressure drop of carbon dioxide is highly dependent on the wettability and pore size distribution of the MPL and GDL. The high carbon dioxide pressure can be utilized to repel liquid and reduce liquid fuel and water crossover through the PEM.
(2) The high capillary pressure within the porous components of MEAs facilitates the transfer of liquid from the channel to the CL. In order to reduce the fuel and water crossover through the PEM, liquid connections between the fuel channel and CL should be reduced.
(3) The pore size distribution and wettability have a much more significant impact on the mass transfer of liquid and vapor than the thickness of components.
(4) DMFCs fed with highly concentrated fuel prefer highly hydrophilic MPLs or a gap between the GDL and CL to reduce liquid transfer from the fuel channel to the CL. Both approaches will build a high-pressure gas layer between the CL and the channel and add liquid flow resistance.
(5) Model results are sensitive to the pore size distribution. The breakthrough pressure and the pressure drop due to gas flow through hydrophilic components with a narrow range of pore size could be very high. It also indicates the importance to minimize the number and size of micro-cracks within the MPL and CL to build up carbon dioxide gas flow resistance.

Acknowledgment

The authors highly appreciate the support by the U.S. Department of Energy's Office of Energy Efficiency and Renewable Energy (EERE) under the Fuel Cell Technologies Office Award Number DE-0008440.

Conflict of Interest

There are no conflicts of interest.

Nomenclature

i = current density (A/cm^2)
p = pressure (Pa)
A = projected area of MEA (m^2)
F = Faraday constant, (96,485 C/mol)
K = absolute permeability of porous media (m^2)
M = molecular weight (kg/mol)
Q = volumetric flowrate of gas (m^3/s)
T = temperature (K)
p_C = capillary pressure (Pa)
v_s = superficial velocity (m/s)
R_u = universal gas constant (J/(mol · K))

Greek Symbols

ε = porosity of the porous media (/)
μ = kinetic viscosity (Pa s)
θ = contact angle (deg)
ρ = density (kg/m^3)
σ = surface tension (N/m)

Subscripts

g = gas phase
H_2O = water
l = liquid phase
MeOH = methanol

References

[1] Joghee, P., Malik, J. N., Pylypenko, S., and O'Hayre, R., 2015, "A +Review on Direct Methanol Fuel Cells—In the Perspective of Energy and Sustainability," MRS Energy Sustain., **2**(1).
[2] Li, X., and Faghri, A., 2013, "Review and Advances of Direct Methanol Fuel Cells (DMFCs) Part I: Design, Fabrication, and Testing With High Concentration Methanol Solutions," J. Power Sources, **226**(15), pp. 223–240.
[3] Alias, M. S., Kamarudin, S. K., Zainoodin, A. M., and Masdar, M. S., 2020, "Active Direct Methanol Fuel Cell: An Overview," Int. J. Hydrog. Energy, **45**(38), pp. 19620–19641.
[4] Shrivastava, N. K., Thombre, S. B., and Chadge, R. B., 2016, "Liquid Feed Passive Direct Methanol Fuel Cell: Challenges and Recent Advances," Ionics, **22**(1), pp. 1–23.
[5] Yang, H., Zhao, T. S., and Ye, Q., 2005, "In Situ Visualization Study of CO2 gas Bubble Behavior in DMFC Anode Flow Fields," J. Power Sources, **139**(1–2), pp. 79–90.
[6] Li, M., Liang, J., Liu, C., Sun, G., and Zhao, G., 2009, "Effects of Anode Flow Field Design on CO2 Bubble Behavior in μDMFC," Sensors, **9**(5), pp. 3314–3324.
[7] Xu, C., He, Y. L., Zhao, T. S., Chen, R., and Ye, Q., 2006, "Analysis of Mass Transport of Methanol at the Anode of a Direct Methanol Fuel Cell," J. Electrochem. Soc., **153**(7), p. A1358.
[8] Meyers, J. P., and Newman, J., 2002, "Simulation of the Direct Methanol Fuel Cell : II. Modeling and Data Analysis of Transport and Kinetic Phenomena," J. Electrochem. Soc., **149**(6), p. A718.
[9] García, B. L., Sethuraman, V. A., Weidner, J. W., White, R. E., and Dougal, R., 2004, "Mathematical Model of a Direct Methanol Fuel Cell," ASME J. Fuel Cell Sci. Technol., **1**(1), pp. 43–48.
[10] Kulikovsky, A. A., 2003, "Analytical Model of the Anode Side of DMFC: the Effect of non-Tafel Kinetics on Cell Performance," Electrochem. Commun., **5**(7), pp. 530–538.
[11] Wang, Y., and Sauer, D. U., 2015, "Optimization of DMFC Regulation Based on Spatial Modeling," Int. J. Hydrog. Energy, **40**(35), pp. 12023–12033.
[12] Miao, Z., Xu, J.-L., and He, Y.-L., 2014, "Modeling of the Transport Phenomena in Passive Direct Methanol Fuel Cells Using a Two-Phase Anisotropic Model," Adv. Mech. Eng., **6**, p. 812706.
[13] García-Salaberri, P. A., and Vera, M., 2016, "On the Effect of Operating Conditions in Liquid-Feed Direct Methanol Fuel Cells: A Multiphysics Modeling Approach," Energy, **113**, pp. 1265–1287.
[14] Jiang, J., Li, Y., Liang, J., Yang, W., and Li, X., 2019, "Modeling of High-Efficient Direct Methanol Fuel Cells With Order-Structured Catalyst Layer," Appl. Energy, **252**, p. 113431.
[15] Wang, Z. H., and Wang, C. Y., 2003, "Mathematical Modeling of Liquid-Feed Direct Methanol Fuel Cells," J. Electrochem. Soc., **150**(4), p. A508.
[16] Su, X., Yuan, W., Lu, B., Zheng, T., Ke, Y., Zhuang, Z., Zhao, Y., Tang, Y., and Zhang, S., 2020, "CO2 Bubble Behaviors and two-Phase Flow Characteristics in Single-Serpentine Sinusoidal Corrugated Channels of Direct Methanol Fuel Cell," J. Power Sources, **450**, p. 227621.
[17] He, Y.-L., Li, X.-L., Miao, Z., and Liu, Y.-W., 2009, "Two-phase Modeling of Mass Transfer Characteristics of a Direct Methanol Fuel Cell," Appl. Therm. Eng., **29**(10), pp. 1998–2008.
[18] Li, X., 2015, "A Modeling Study of the Pore Size Evolution in Lithium-Oxygen Battery Electrodes," J. Electrochem. Soc., **162**(8), pp. A1636–A1645.
[19] Inoue, G., Yokoyama, K., Ooyama, J., Terao, T., Tokunaga, T., Kubo, N., and Kawase, M., 2016, "Theoretical Examination of Effective Oxygen Diffusion Coefficient and Electrical Conductivity of Polymer Electrolyte Fuel Cell Porous Components," J. Power Sources, **327**, pp. 610–621.
[20] Miao, Z., Zihang, L., Yaling, H., Jinliang, X., and Xianglin, L., "A Liquid-Vapor Two-Phase Model of Direct Methanol Fuel Cells With PGM-Free Cathode Catalyst," Energy, Under Review.
[21] Kozbial, A., Trouba, C., Liu, H., and Li, L., 2017, "Characterization of the Intrinsic Water Wettability of Graphite Using Contact Angle Measurements: Effect of Defects on Static and Dynamic Contact Angles," Langmuir, **33**(4), pp. 959–967.
[22] Goswami, S., Klaus, S., and Benziger, J., 2008, "Wetting and Absorption of Water Drops on Nafion Films," Langmuir, **24**(16), pp. 8627–8633.
[23] Duan, Q., Wang, H., and Benziger, J., 2012, "Transport of Liquid Water Through Nafion Membranes," J. Membr. Sci., **392–393**, pp. 88–94.
[24] Vazquez, G., Alvarez, E., and Navaza, J. M., 1995, "Surface Tension of Alcohol Water + Water From 20 to 50. Degree.C," J. Chem. Eng. Data, **40**(3), pp. 611–614.
[25] Li, X., Miao, Z., Marten, L., and Blankenau, I., 2020, "Experimental Measurements of Fuel and Water Crossover in an Active DMFC," Int. J. Hydrog. Energy, **46**(5), pp. 4437–4446.
[26] Kim, H., Lim, J.-H., Lee, K., and Choi, S. Q., 2020, "Direct Measurement of Contact Angle Change in Capillary Rise," Langmuir, **36**(48), pp. 14597–14606.
[27] Xu, C., Faghri, A., and Li, X., 2010, "Development of a High Performance Passive Vapor-Feed DMFC Fed With Neat Methanol," J. Electrochem. Soc., **157**(8), pp. B1109–B1117.
[28] Sun, J., Zhang, G., Guo, T., Che, G., Jiao, K., and Huang, X., 2020, "Effect of Anisotropy in Cathode Diffusion Layers on Direct Methanol Fuel Cell," Appl. Therm. Eng., **165**, p. 114589.